Gene 689 (2019) 227–234

Contents lists available at ScienceDirect

Gene

journal homepage: www.elsevier.com/locate/gene

Short communication

Characterization of two novel mutations in the claudin-16 and claudin-19 genes that cause familial hypomagnesemia with hypercalciuria and nephrocalcinosis

Ana Perdomo-Ramirez[a], Mireia Aguirre[b], Tinatin Davitaia[c], Gema Ariceta[d], Elena Ramos-Trujillo[a], RenalTube Group, Felix Claverie-Martin[a,*]

[a] Unidad de Investigacion, Hospital Nuestra Señora de Candelaria, Santa Cruz de Tenerife, Spain
[b] Nefrologia Pediatrica, Hospital de Cruces, Baracaldo, Spain
[c] Paediatric Nephrology, M. Iashvili Childrens Hospital, Tbilisi, Georgia
[d] Nefrologia Pediatrica, Hospital Vall d' Hebron, Barcelona, Spain

ARTICLE INFO

Keywords:
CLDN16
CLDN19
Hypomagnesemia
Hypercalciuria
Nephrocalcinosis
Mutation
Minigene
Pre-mRNA splicing
Exon skipping
Claudin

ABSTRACT

Familial hypomagnesemia with hypercalciuria and nephrocalcinosis is an autosomal-recessive renal tubular disorder characterized by excessive urinary losses of magnesium and calcium, bilateral nephrocalcinosis and progressive chronic renal failure in childhood or adolescence. The disease is caused by mutations in the tight-junction proteins claudin-16 and claudin-19 that are encoded by the *CLDN16* and *CLDN19* genes, respectively. Patients with *CLDN19* mutations also are affected with severe ocular abnormalities. The aim of our study was to identify and characterize the molecular defects causing this disease in a Georgian girl and two Spanish siblings. Clinical and biochemical parameters were studied. The *CLDN16* and *CLDN19* genes were analyzed by DNA sequencing. The functional consequences of the identified mutations on pre-mRNA splicing were investigated using a minigene assay. Sequence analysis revealed that the patient from Georgia was homozygous for a novel mutation, c.602G > A; p.(G201E), in exon 4 of the *CLDN16* gene. The two Spanish siblings were homozygous for a new *CLDN19* mutation, c.388G > T; p.(G130C), located in exon 2, and both parents were heterozygous carriers of the mutation. Bioinformatics analysis predicted that the amino acid substitutions generated by these mutations were pathogenic. Functional studies showed that mutation c.388G > T also results in partial skipping of *CLDN19* exon 2, which would imply significant alterations in the claudin-19 protein structure. Conversely, *CLDN16* mutation c.602G > A had no effect on pre-mRNA splicing. Our study expands the genotypic classification of this rare disease and provides the first report of a *CLDN19* mutation affecting splicing.

1. Introduction

Familial hypomagnesemia with hypercalciuria and nephrocalcinosis (FHHNC) is a rare autosomal recessive tubulopathy characterized by excessive excretion of renal magnesium and calcium, bilateral severe nephrocalcinosis, progression to chronic renal failure during childhood or adolescence, and, in a subset of patients, ocular abnormalities (Michelis et al., 1972; Praga et al., 1995; Claverie-Martin, 2015). More recently, it has been reported that FHHNC patients have defects in enamel formation (Bardet et al., 2016; Yamaguti et al., 2017). Patients typically present with polyuria, polydipsia, recurrent urinary tract infections (UTI), failure to thrive, and muscular tetany. Frequent laboratory findings include hypomagnesemia, hypercalciuria, high serum levels of intact parathyroid hormone (PTH), hypocitraturia, and decreased glomerular filtration rate (GFR) (Godron et al., 2012; Konrad et al., 2008; Weber et al., 2001). In some patients with advanced chronic kidney disease (CKD), hypomagnesemia may be overlooked (Claverie-Martin, 2015). Thus, the presence of hypomagnesemia is not

Abbreviations: bp, base pairs; FHHNC, Familial hypomagnesemia with hypercalciuria and nephrocalcinosis; CKD, chronic kidney disease; CL, cytoplasmic loop; ECL, extracellular loop; ESE, exonic splicing enhancer; ESRD, end-stage renal disease; FE Mg, fractional excretion of magnesium; GFR, glomerular filtration rate; HGMD, Human Gene Mutation Database; HSF, Human Splicing Finder; MWM, molecular weight marker; NCBI, National Center for Biotechnology Information; nt, nucleotides; PCR, polymerase chain reaction; PTH, intact parathyroid hormone; RT-PCR, reverse transcription-PCR; TGP, 1000 Genomes Project; TJ, tight junction; TMD, transmembrane domain; UTI, urinary tract infections; WT, wild-type

* Corresponding author at: Unidad de Investigación, Hospital Nuestra Señora de Candelaria, Carretera del Rosario 145, 38010 Santa Cruz de Tenerife, Spain.
E-mail address: fclamar@gobiernodecanarias.org (F. Claverie-Martin).

https://doi.org/10.1016/j.gene.2018.12.024
Received 10 October 2018; Received in revised form 3 December 2018; Accepted 14 December 2018
Available online 18 December 2018
0378-1119/

always required for the diagnosis. Additionally, detection of more severe hyperparathyroidism than expected for CKD stage is characteristic of the disease. Due to the autosomal-recessive mode of inheritance, a substantial fraction of affected patients originate from populations with high frequency of consanguineous parents. The only current treatment for renal dysfunction in FHHNC patients is transplantation in end-stage renal disease (ESRD) (Praga et al., 1995). Supportive therapy with supplementation of magnesium and the use of thiazide diuretics simply delay the onset of ESRD (Weber et al., 2001).

FHHNC disease is caused by loss-of-function mutations in *CLDN16* (FHHNC type 1, MIM #248250) or *CLDN19* (FHHNC type 2, MIM #248190) (Simon et al., 1999; Konrad et al., 2006). These genes are expressed in the kidney and encode tight-junction proteins claudin-16 and claudin-19, respectively, which are responsible for the cation selectivity of the tight junctions (TJ), and thus are involved in the regulation of paracellular reabsorption of magnesium and calcium along the thick ascending limb (TAL) of Henle's loop (Simon et al., 1999; Blanchard et al., 2001; Konrad et al., 2006; Hou et al., 2008). Claudin-19 is also highly expressed in retina, consequently patients with mutations in *CLDN19* additionally present severe ocular defects such as myopia, nystagmus and macular colobamata (Konrad et al., 2006; Claverie-Martín et al., 2013; Godron et al., 2012). Claudin-16 and claudin-19 contain four transmembrane domains (TMD 1–4), two extracellular loops (ECL 1–2), a cytoplasmic loop (CL), and cytoplasmic amino- and carboxy termini (Claverie-Martin, 2015).

Until now, a total 68 different *CLDN16* mutations and 19 *CLDN19* mutations have been reported according to the Human Gene Mutation Database (HGMD, Stenson et al., 2017). A genotype-phenotype correlation related to the progression of renal failure in FHHNC patients with *CLDN16* mutations has been proposed (Konrad et al., 2008). Nevertheless, the pathophysiology of this disease remains unclear. Hypercalciuria and nephrocalcinosis may contribute to the frequent progression to end stage kidney disease, but an abnormal developmental tubular defect has been suggested (Godron et al., 2012). In the present study, we report two Spanish siblings and a Georgian girl with FHHNC caused by novel homozygous mutations in *CLDN19* and *CLDN16*, respectively. We also describe the functional consequences of these novel mutations on pre-mRNA splicing.

2. Patients and methods

2.1. Clinical tests

Serum and urine levels of calcium, magnesium and creatinine were analyzed using standard laboratory methods in the central laboratories of the respective hospitals. Hypomagnesemia was defined when serum magnesium levels were maintained below 1.6 mg/dl. Renal magnesium loss was considered excessive when fractional excretion of magnesium (FE Mg) % value was > 4%. Urinary calcium levels above 4 mg/kg/day were considered as hypercalciuria. GFR was estimated from serum creatinine using the Schwartz formula (Schwartz et al., 2009); GFR levels below 90 ml/min/1,73 m^2 were considered as CKD. Bilateral nephrocalcinosis was detected by ultrasound or radiography. Ophthalmologic exploration was performed in the Ophthalmology Services of the respective hospitals.

2.2. Case description

Two patients from Spain and one from Georgia were clinically diagnosed with FHHNC at the Paediatric Nephrology Services of Cruces University Hospital (Baracaldo) and M. Iashvili Children's Central Hospital (Tbilisi), respectively.

Patient 1 (index case) was a 4-year-old boy from a consanguineous Spanish family (great-grandparents were cousins). He was referred for renal studies after a fortuitous finding of hypertension and severe hypercalciuria (14.47 mg/kg/day, normal range < 4 mg/kg/day). He was born at term without complications and had no history of UTI. His parents reported polydipsia and polyuria. Abdominal ultrasound revealed medullary nephrocalcinosis. He had suffered an atypical febrile seizure at 15 months of age. His physical and psychomotor developments were normal. At the age of 3 years he was diagnosed with myopia magna. Later studies showed hypomagnesemia (1.31 mg/dl, normal range 1.6–2.6 mg/dl) with elevated fractional excretion rate of magnesium (FE Mg, 10.6%; normal range < 4%), hypercalciuria (9.9 mg/kg/day), hypocitraturia (103 mg/day, normal range 300–600 mg/day), and elevated levels of PTH in serum (106 pg/ml; normal range 10–65 pg/ml). Renal ultrasound revealed bilateral nephrocalcinosis. The clinical data, together with the laboratory findings and the imaging studies were consistent with FHHNC (type 2). The patient is now 13 years old and is followed-up at the outpatient clinic with regular analytical controls and kidney ultrasound scans. His renal function is progressively deteriorating (current GFR: 42 mls/min/1,73 m^2). He occasionally presents paraesthesia, unrelated to physical exercise.

His 15-year-old brother, Patient 2, was followed since he was 8 years old after being diagnosed of FHHNC by family screening due his sibling diagnosis. He was born at term without complications. Parents reported polydipsia and polyuria since childhood. No other neonatal history was relevant. He was diagnosed of myopia magna and macular colobomata as well. He suffered abdominal pain occasionally. Preliminary laboratory test showed a serum magnesium concentration of 1.47 mg/dl and high fractional excretion of magnesium (21%). Urinary analysis also revealed hypercalciuria (6 mg/kg/day), hypocitraturia (189 mg/day; normal range 300–600 mg/day) and a low estimated GFR of 60 mls/min/1.73 m^2. At that time, abdominal X-rays demonstrated bilateral nephrocalcinosis. These clinical findings were consistent with FHHNC (type 2). Currently, he shows progressive renal failure (GFR: 46 mls/min/1.73 m^2), moderate hypercalciuria between 4.3 and 6 mg/kg/day, whereas serum magnesium persists between 1.16 and 1.47 mg/dl. Both brothers are being managed with thiazide diuretics and vitamin D, and oral magnesium and citrate supplementation.

Patient 3 was a two months old girl from Georgia who was admitted to the hospital with hypovolemic shock and seizures. She was born at term. History was remarkable for periodic vomiting, polyuria, and failure to thrive. No UTI were reported. Initial tests revealed profound hypomagnesemia (serum magnesium: 1 mg/dl) and bilateral medullary nephrocalcinosis. Further laboratory tests confirmed hypercalciura (10 mg/kg/day), hypermagnesuria (FE Mg 13.89%) and hypocitraturia (7.66 mg/day). Family history was positive for nephrolithiasis (parents and male grandparents). No eyes anomalies were reported. On the basis of this laboratory and imaging studies the diagnosis of FHHNC was established. Genetic analysis confirmed FHHNC type 1. The patient is now 2.8 years old and is on magnesium supplementation. Her estimated GFR is low (62.9 mls/min/1.73 m^2).

2.3. Ethical compliance

Informed written consent for the genetic analysis was obtained from the patients' parents. The Ethics Committee of Nuestra Señora de Candelaria University Hospital (Santa Cruz de Tenerife, Spain) approved this study.

2.4. Mutation analysis

Blood and urine samples were collected for biochemical and genetic analysis. Genomic DNA of patients and relatives was extracted from peripheral blood samples using the GenElute Blood Genomic DNA kit (Sigma-Aldrich, St. Louis, MO, USA) following the manufacturer's instructions. The DNA sample of the patient from Georgia was spotted onto a Whatman FTA classic card (GE Healthcare Life Sciences, Buckinghamshire, UK) and stored at room temperature for preservation. Small punched disks were removed from the sample card and

washed with the FTA Purification Reagent (GE Healthcare Life Sciences) according to the manufacturer's protocol. Genomic DNA was then amplified using the illustra Ready-To-Go GenomiPhi V3 DNA Amplification kit (GE Healthcare Life Sciences). The coding exons and the flanking intronic sequences of *CLDN16* and *CLDN19* were amplified by polymerase chain reaction (PCR) using intronic primers previously described (Claverie-Martín et al., 2013; Simon et al., 1999). PCR products were purified with the QIAquick PCR purification kit (Qiagen, Hilden, Germany) and sequenced with the BigDye Terminator v3.1 Cycle Sequencing Kit (Applied Biosystems, Foster City, CA, USA). Sequence reactions were purified with Performa® DTR Gel Filtration Cartridges (EdgeBio BioSystems, Gaithersburg, Maryland, USA), and analyzed on a 3500 Series Genetic Analyzer (Applied Biosystems, Foster City, CA, USA). Mutations were identified by comparison to the respective reference sequences (GeneBank accession numbers NG_008993.1 and NG_008149.1, for *CLDN19* and *CLDN16*, respectively), and confirmed by sequencing additional independent amplification products.

2.5. Bioinformatics analysis of mutations

The potential effect of amino acid substitutions on the structure and function of claudin-16 and claudin-19 proteins was evaluated using the bioinformatics tools SIFT (http://sift.bii.a-star.edu.sg/www/SIFT_seq_submit2.html) (Sim et al., 2012), PolyPhen-2 (http://genetics.bwh.harvard.edu/pph2/) (Adzhubei et al., 2010), Align GVGD (http://agvgd.iarc.fr/) (Tavtigian et al., 2006) and MutPred2 (http://mutpred.mutdb.org/) (Pejaver et al., 2017). NNSplice version 0.9 of the Splice Site Prediction by Neural Network was used to evaluate the effect of mutations on splice sites (http://www.fruitfly.org/seq_tools/splice.html) (Reese et al., 1997). Human Splicing Finder v3.1 (HSF) was used to predict the effect of mutations on exonic splicing enhancers (http://www.umd.be/HSF3/) (Desmet et al., 2009). Default settings were used for all programs.

2.6. Minigene construction and splicing assays

To evaluate the effect of mutations on *CLDN16* and *CLDN19* pre-mRNA splicing we used a minigene system and reverse transcription-PCR (RT-PCR) analysis. For the construction of the *CLDN19* minigenes, a fragment of 676 containing exons 2 and 3 and the flanking intronic sequences was PCR amplified from genomic DNA of a control and patient 1 using specific primers and a high fidelity DNA polymerase (KAPA HiFi PCR kit, KAPA Biosystems Inc., MA, USA). The forward (5′-TTGTCTCGAGTGAAGGGGACTCTCAC-3′) and reverse (5′-TTCCTCTAGAAAGCTTCTTGGACAGC-3′) primers contained restriction sites for *Xho*I, and *Xba*I, respectively, at their 5′ ends (underlined). After restriction digestion, the PCR products were cloned into the *Xho*I/*Xba*I-digested pET01 expression vector (MoBITec, Göttingen, Germany). The insert had the following structure: 3′ end of intron 1 (203 bp) – exon 2 (165 bp) – intron 2 (107 bp) – exon 3 (85 bp) – 5′ end of intron 2 (116 bp). Mutation c.389G > A, identified by Naeem et al. (2011), was introduced in the wild-type (WT) minigene by site-directed mutagenesis using primers 5′-CAGTCAAAGTGCAGAGGTCTAAAGACAAAGCAGAG-3′, and 5′-CTCTGCTTTGTCTTTAGACCTCTGCACTTTGACTG-3′ (the altered nucleotides are underlined) and the Quik-Change II Site-Directed Mutagenesis Kit (Agilent Technologies, Santa Clara, CA, USA) following the manufacturer's instructions. Control and mutant *CLDN16* minigenes were constructed by inserting into the digested pET01 vector a fragment of 689 bp that corresponds to *CLDN16* exon 4 (192 bp) and the flanking 5′ and 3′ intronic sequences (261 bp and 236 bp, respectively) with the WT or mutant sequences. These fragments were amplified by PCR using genomic DNA from a healthy control or patient 3, forward primer 5′-ATTCTCGAGGATTTACACAGATAAGCAC-3′, and reverse primer 5′-ACGTCTAGAATTTGAATATTGGACATGC-3′, containing restriction sites for *Xho*I, and *Xba*I, respectively, at their 5′ ends (underlined). The fidelity of the inserts was confirmed by DNA sequencing.

Minigenes were transfected into COS7 cells using JetPRIME® (Polyplus Tranfection, Illkirch, France), according to the manufacturer's instructions. RNA was extracted after incubation for 48 h and purified using the High Pure RNA Isolation Kit (Roche, Basel, Switzerland). RT-PCR was carried out as previously described (Suarez-Artiles et al., 2018). Products were separated by electrophoresis in 1.5% agarose gels. As molecular weight marker we used the PCR 100 bp Low Ladder (Sigma-Aldrich). DNA bands were visualized in a Gel Doc EZ Imager (Bio-Rad) after staining with GelRed (Biotoium, Inc., Fremont, CA, USA), and were recovered from the agarose gels using the GenElute™ Gel Extraction Kit (Sigma-Aldrich) and analyzed by DNA sequencing.

2.7. Protein structure prediction

The three-dimensional structure of human WT and mutant claudin-19 proteins was predicted with the Iterative Threading ASSEmbly Refinement (I-TASSER) server version 5.1 (https://zhanglab.ccmb.med.umich.edu/I-TASSER/) (Roy et al., 2010; Yang et al., 2015) using the amino acid sequences of the proteins. The NCBI accession number of the amino acid sequences for claudin-19 was NP_683763.

3. Results

DNA sequencing of the five coding exons and intron-exon boundaries of *CLDN19* amplified from genomic DNA of patients 1 and 2 revealed a novel homozygous mutation in exon 2, which consisted in the substitution of a G for a T in codon 130 predicting a change of glycine for cysteine [c.388G > T; p.(G130C); chr1:43204092C > A; Ensembl transcript ID: ENST00000296387.5, Fig. 1A]. The mutation was confirmed by bidirectional sequencing of an independent PCR product. As expected, both parents were heterozygous carriers of the mutation (Fig. 1A and B). This new *CLDN19* variant was not annotated in databases such as the Exome Aggregation Consortium (ExAC), 1000 Genomes Project (TGP), HGMD and ClinVar. The glycine residue of the claudin-19 protein affected by this mutation is evolutionary highly conserved among vertebrate species (Fig. 1C). Bioinformatics analysis of the amino acid change (glycine to cysteine) resulting from this mutation showed that it affects protein function (Table 1).

Since mutation c.388G > T is located in the last nucleotide of *CLDN19* exon 2, we assumed that it could also alter the donor splice site of intron 2. Therefore, we analyzed it with NNsplice, a bioinformatics tool that predicts and evaluates splice sites in genes. The results showed that the G to T change lowered the NNsplice score of the donor splice site of intron 2 from 0.99 in the WT to 0.78 in the mutant. To functionally confirm whether this variant disrupted splicing, we constructed minigenes with an insert corresponding to *CLDN19* exons 2 and 3 and the flanking intronic sequences, and containing the mutation or the WT sequence (Fig. 2B). After transfection and incubation, the RNA was purified and the effect on splicing determined by RT-PCR analysis and sequencing. The results with the WT *CLDN19* minigene revealed the expected canonical transcript of 487 nt [5′ pET01 exon (178 nt) + CLDN19 exons 2 (165 nt) and 3 (85 nt) + 3′ pET01 exon (59 nt)] (Fig. 2A). However, the minigene with mutation c.388G > T produced two transcripts, one corresponding to the canonical transcript and another of 322 nt containing only exon 3 joined to the two pET01 exons [5′ pET01 exon (178 nt) + CLDN19 exon 3 (85 nt) + 3′ pET01 exon (59 nt)] (Fig. 2). Therefore, mutation c.388G > T induced skipping of exon 2. This exon contains 165 nucleotides and encodes 55 amino acids of the WT claudin-19 protein, which is composed of 224 amino acids (Konrad et al., 2006). Consequently, the shorter *CLDN19* transcript generated by mutation c.388G > T would encode a claudin-19 protein lacking a small portion of ECL1, the entire TMD2, the cytoplasmic loop between TMD2 and TMD3, and approximately half of TMD3. Fig. 2C shows the three-dimensional structure predictions of this

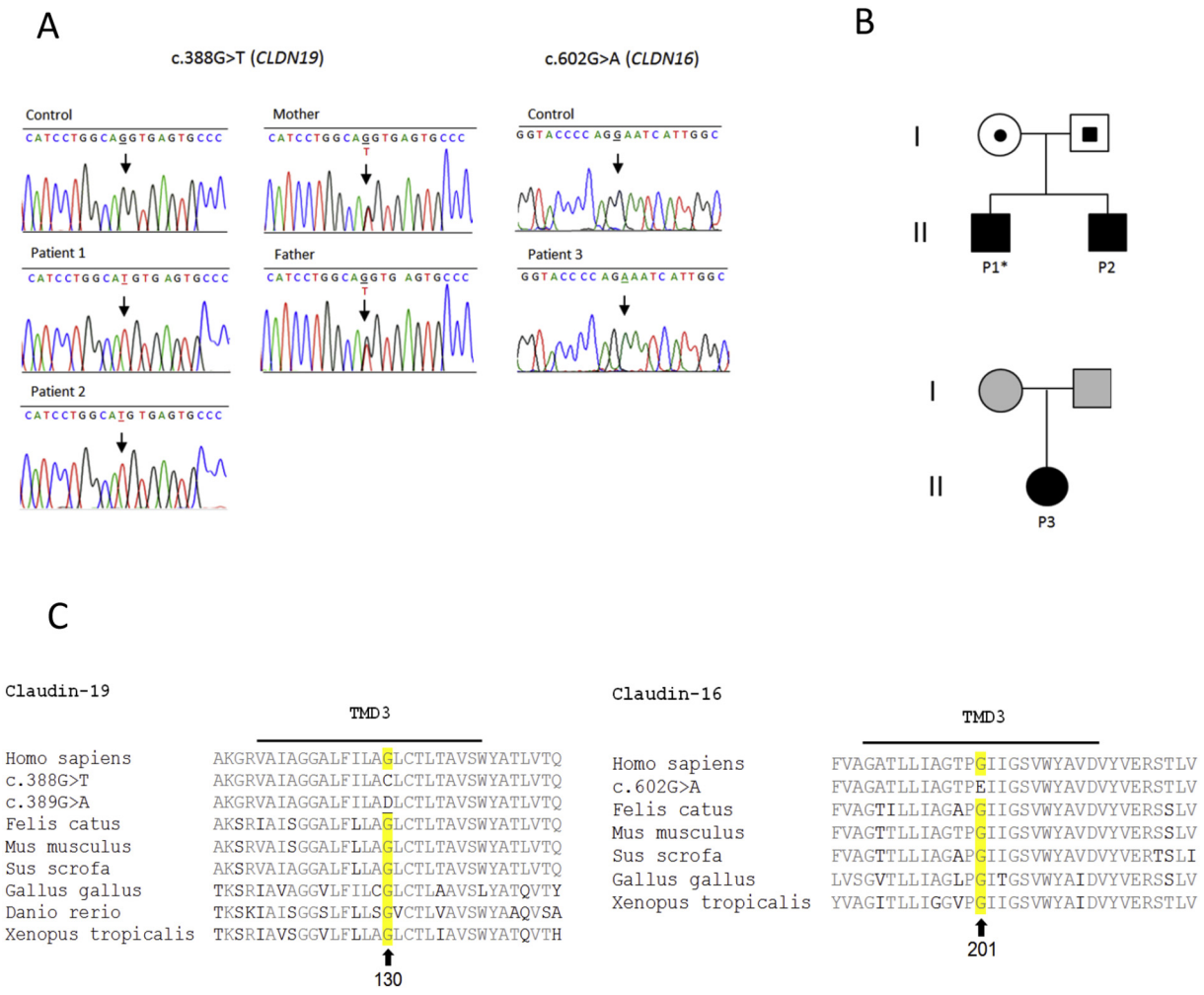

Fig. 1. Novel mutations identified in FHHNC patients, family pedigrees and multiple sequence alignments. (A) DNA sequence analysis of *CLDN19* in patients 1 and 2 (Family I) revealed homozygous mutation c. 388G > T. Both parents were heterozygous carriers. Mutation analysis of *CLDN16* identified homozygous substitution c.602G > A in patient 3 (Family II). Arrows indicate the affected nucleotides. (B) Pedigree of FHHNC families 1 and 2. Circles and squares represent female and male individuals, respectively; black circles and squares represent homozygous patients; black circles and squares within open frames denote heterozygous parents; grey symbols represent family members who were not available for genetic analysis. Index patients are designated with an asterisk. Families I and II have mutation in *CLDN19* and *CLDN16*, respectively. (C) Multiple alignment analysis showed conservation of glycine 130 and glycine 201 (in yellow) among claudin-19 and claudin-16 proteins, respectively. These amino acid residues are both located in transmembrane domain 3 (TMD3, black bar) of the respective claudin protein. Grey and black letters represent conserved and non-conserved residues, respectively. (For interpretation of the references to colour in this figure legend, the reader is referred to the web version of this article.)

altered claudin-19 protein together with the WT generated with the I-TASSER server. For comparison, we also examined the effect on splicing of *CLDN19* mutation c.389G > A, previously described as missense mutation p.(G130D) in a Pakistani patient with FHHNC. This mutation affects the same codon as c.388G > T but is located in the first nucleotide of *CLDN19* exon 3 (Fig. 2) (Naeem et al., 2011). Analysis with NNsplice suggested that c.389G > A essentially did not alter the score of the acceptor splice site of intron 3 (from 0.98 in the WT to 0.94 in the mutant). In agreement with this, the results of our minigene analysis showed that mutation c.389G > A did not affect pre-mRNA splicing (Fig. 2).

Mutation analysis of patient 3 identified a homozygous mutation in exon 4 of *CLDN16*, consisting in a G to A substitution in codon 201 that predicts the change of glycine for glutamic acid [c.602G > A; p.(G201E); chr3:190126112G > A; Ensembl transcript ID: ENST00000264734.2, Fig. 1A]. The mutation was confirmed by sequencing of an independent PCR product, but unfortunately we were not able to extend the genetic testing to the patient's parents. This variant had not been reported in the literature and was not registered in the ExAC, TGP, HGMD and ClinVar databases. The affected amino acid residue, Glycine 201, is highly conserved among vertebrate species (Fig. 1C). Analysis with bioinformatics tools PolyPhen, Align GVGD and MutPred of the amino acid change predicted for this mutation suggested that it is pathogenic, although according to SIFT it is tolerated (Table 1). Mutation c.602G > A is located nine nucleotides downstream from the acceptor splice site of intron 3 but it does not affect its NNsplice score (from 0.99 in WT to 0.98 in mutant). As the mutation is nearby the 5′ end of exon 4, we analyzed it with the *in silico* tool HSF to determine if it potentially affected an exonic splicing enhancer (ESE). The results suggested that c.602G > A alters an ESE site with potential change of pre-mRNA splicing. To confirm whether this mutation disrupted splicing experimentally, we constructed minigenes containing *CLDN16* exon 4 and its flanking intronic sequences with both the WT sequence and mutant sequence. The RT-PCR analysis revealed that both WT and mutant *CLDN16* minigenes produced the same two bands, a major one of approximately 450 bp that contained *CLDN16* exon 4 plus the two exons from pET01, and a minor one that was missing exon 4 (Fig. 3). The mutation seemed to decrease slightly the level of the minor band. Therefore, we concluded that mutation c.602G > A does not induce skipping of exon 4 in the minigene system.

Table 1
Bioinformatics predictions of the amino acid changes caused by mutations.

Mutation	SIFT (score)[a]	PolyPhen-2 (score)[b]	Align GVGD (class)[c]	MutPred2 (score)[d]
p.G201E	Tolerated (0.14)	Probably damaging (1.000)	Interferes with function (C65)	Deleterious (0.651)
p.G130C	Affects function (0.00)	Possibly damaging (0.732)	Interferes with function (C65)	Deleterious (0.676)
p.G130D	Affects function (0.00)	Possibly damaging (0.921)	Interferes with function (C65)	Deleterious (0.881)

[a] The SIFT probability score ranges from 0 to 1.0. Amino acid substitutions with scores < 0.05 are predicted to be deleterious (scores closer to 0 are more confidently predicted to be deleterious). Variants with scores in the range 0.05 to 1.00 are predicted to be tolerated (scores very close to 1.0 are more confidently predicted to be tolerated).

[b] The PolyPhen-2 score ranges from 0.0 to 1.0. Values closer to 1.0 are more confidently predicted to be deleterious. Variants with scores in the range 0.0 to 0.15 are predicted to be benign, while variants with scores in the range 0.15 to 1.0 are possibly damaging. Variants with scores in the range 0.85 to 1.0 are more confidently predicted to be damaging.

[c] Align-GVGD classifies variants in seven risk grades (C0, C15, C25, C35, C45, C55, C65) with C65 most likely to interfere with function and C0 least likely.

[d] The general score of MutPred2 ranges from 0.0 and 1.0, with a higher score indicating a greater propensity to be pathogenic.

The new variants, *CLDN16* c.602G > A and *CLDN19* c.388G > T, have been deposited in the ClinVar database (https://www.ncbi.nlm.nih.gov/clinvar/submitters/505967/), and are now listed with ID numbers 560390 and 560599, respectively.

4. Discussion

Claudins are important structural and functional components of the TJ that form paracellular diffusion barriers and pores and regulate epithelial permeability of small molecules and water (Tsukita and Furuse, 2000; Günzel and Yu, 2013). Claudin-16 and claudin-19 are expressed in the TAL and form an essential complex that is involved in the regulation of paracellular reabsorption of magnesium and calcium in the kidney (Simon et al., 1999; Hou et al., 2008, 2009). Claudin-19 is also expressed in retinal epithelium and peripheral neurons (Konrad et al., 2006; Miyamoto et al., 2005). Mutations in the gene that encodes claudin-16, *CLDN16*, cause FHHNC, while mutations in the gene encoding claudin-19, *CLDN19*, caused the same phenotype together with severe ocular defect (Simon et al., 1999; Konrad et al., 2006). The function of claudin-19 in the peripheral nervous system remains elusive. *Cldn19* knockout mice exhibit behavioral abnormalities resembling a peripheral neuropathy and lack TJ structures in Schwann cells (Miyamoto et al., 2005). Claudin-16 and claudin-19 are also expressed in the TJ of ameloblast, and loss-of-function mutations in the encoding genes are associated with amelogenesis imperfecta (Bardet et al., 2016; Yamaguti et al., 2017).

In general, mutations in *CLDN16* are responsible for most FHHNC cases reported so far. These are mainly missense mutations, and a few nonsense mutations, splice site mutations, deletions and insertions (Simon et al., 1999; Weber et al., 2000, 2001; Müller et al., 2003; Hampson et al., 2008; Godron et al., 2012; Hanssen et al., 2014; Claverie-Martín et al., 2015). The most common *CLDN16* mutation is c.453G > T, p.(L151F), which appears in approximately half of the patients from Germany and Eastern Europe (Weber et al., 2001). Another recurrent *CLDN16* mutation detected in patients from North Africa is p.(A139V) (Godron et al., 2012). In Spain and the south of France, most patients present *CLDN19* homozygous mutation p.(G20D) that is also due to a founder effect (Konrad et al., 2006; Godron et al., 2012; Claverie-Martín et al., 2013; Martin-Nuñez et al., 2015). According to the HGMD, no splice site mutations have been identified in *CLDN19*. Although two mutations located in the last nucleotide of exon 1 that reduce the strength of the donor splice site and could affect *CLDN19* splicing have been reported (Claverie-Martín et al., 2013).

Here, we investigated the genotypes of two patients from a consanguineous Spanish family and one patient from Georgia diagnosed with FHHNC. These patients exhibited the usual clinical and biochemical characteristics of FHHNC, including polydipsia/polyuria, hypomagnesemia, hypermagnesuria, hypercalciuria, hypocitraturia, bilateral nephrocalcinosis and decreased GFR. The Spanish siblings, who also had severe ocular defects, were homozygous for a novel *CLDN19* mutation, c.388G > T. This mutation predicts the deleterious substitution of glycine for cysteine in residue 130 of claudin-19, p.(G130C), affecting TMD3 of the claudin-19 protein. On the other hand, c.388G > T is located in the last nucleotide of exon 2, and bioinformatics analysis indicated that it reduces the strength of the donor splice site of intron 2. This suggested that the mutation could also affect the pre-mRNA splicing process in *CLDN19*. To confirm this, we performed a functional analysis using a minigene system. The ideal RNA source for functional assays would be RNA from patients' kidneys but in this case it was not available. An alternative approach is to use splicing reporter minigenes since several studies have shown a high degree of concurrence between the results obtained with them and those obtained with patients' RNA (Tournier et al., 2008; Steffensen et al., 2014; van der Klift et al., 2015). The results of our functional assay showed that the novel mutation, c.388G > T, altered in part the splicing of the *CLDN19* pre-mRNA by inducing the skipping of exon 2. The mechanism of the exon skipping seems to be the alteration of the donor splice site as it has been reported for other exonic mutations (Gonzalez-Paredes et al., 2016; de Calais et al., 2017; Suarez-Artiles et al., 2018). The altered transcripts would encode a claudin-19 protein with important 3-dimensional structure modifications as predicted by the I-TASSER server. On the other hand, the transcript with the normal size contains the mutation c.388G > T, and would encode the protein with the corresponding amino acid change, p.(G130C). Therefore, we suggest that *CLDN19* mutation c.388G > T results in a splicing defect and involves two pathogenic mechanisms; one related to the amino acid substitution of a conserved glycine residue for cysteine in TMD3, and another associated to the skipping of exon 2. A similar *CLDN19* mutation affecting the same codon but a different nucleotide, c.389G > A, p.(G130D) has been reported by Naeem et al. (2011) in a Pakistani patient with FHHNC type 2. This mutation also disturbs TMD3 of claudin-19. Based on informatics analysis, they predicted that c.389G > A causes loss of claudin-19 protein function by affecting the heteromeric interaction with claudin-16. Interestingly, this mutation is located in the first nucleotide of exon 3 so we reasoned that it might also affect the acceptor splice site. However, our bioinformatics and functional analysis indicated that mutation c.389G > A does not alter the splicing of the pre-mRNA.

The FHHNC patient from Georgia was homozygous for a novel mutation, c.602G > A; p.(G201E), in *CLDN16*. At the protein level, this mutation affects a conserved glycine residue at position 201 located in TMD3 of claudin-16. Although this mutation alters an exonic splicing enhancer, our minigene analysis indicated that it does not affect pre-mRNA splicing of *CLDN16*. Three pathogenic mutations affecting the TMD3 of claudin-16, p.(G191R), p.(G198A) and p.(G198D), have been previously reported (Simon et al., 1999; Weber et al., 2001). Hou and colleagues have shown that claudin-16 and claudin-19 associate through heteromeric interactions providing the cation selectivity to the TJ in a synergistic manner (Hou et al., 2008). They also indicated that claudin-16 mutant p.(G191R) disrupts this interaction abolishing the synergistic effect. The pathogenic character of the amino acid change predicted for mutation c.602G > A, would have to be confirmed by functional analyses. But, taking into account the severity of the disease and the bioinformatics predictions, we suggest that the substitution of

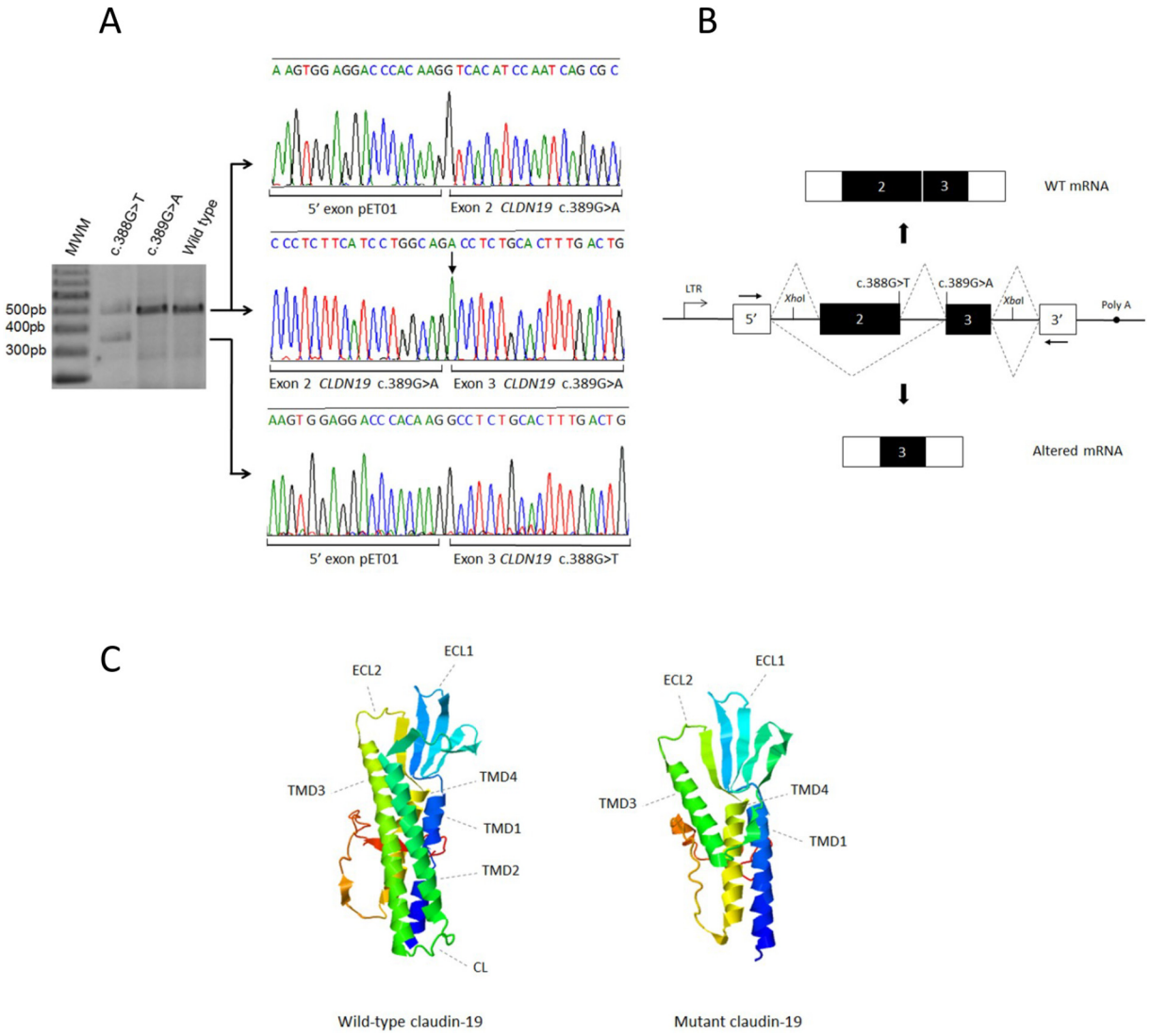

Fig. 2. Functional characterization of *CLDN19* exonic mutations c.388G > T and c.389G > A using a splicing minigene assay. (A) Representative agarose gel showing the results of the RT-PCR analysis of spliced transcripts expressed from *CLDN19* minigenes containing WT and mutant exons. Mutation c.388G > T generated an mRNA product of the same size as the WT together with a smaller product, while mutation c.389G > A produced only the WT product. DNA sequencing results of the different RT-PCR products are shown on the right panel. The electropherogram on the bottom reveals that the altered mRNA product produced by mutant c.388G > T is missing exon 2. The electropherogram in the middle shows the normal joining of exons 2 and 3 in the transcript generated by mutant c.389G > A. The arrow indicates mutation c.389G > A. The electropherogram on the top shows the expected correct joining of 5′ exon from vector pET01 with *CLDN19* exon 2 from mutant c.389G > A. MWM, molecular weight marker. (B) Schematic representation of *CLDN19* minigene and of pre-mRNA splicing in both WT and mutants minigenes. Black and white boxes represent *CLDN19* exons and pET01 exons, respectively. The position of both mutations is indicated together with the restriction sites used for the construction of the minigenes. Arrows above and below the white boxes represent primers used in the RT-PCR assays. Dotted lines indicate the splice sites used in each case. The pET01 vector contains the long terminal repeat promoter (LTR) of Rous sarcoma virus and a polyadenylation site (Poly A). (C) I-TASSER 3-dimensional models for WT claudin-19 and the mutant protein generated by *CLDN19* transcript missing exon 2. The mutant protein lacks the whole TMD2, the cytoplasmic loop (CL) and approximately half of TMD3.

glycine for cysteine also results in loss of claudin-16 function, and that the pathogenic mechanism for development of FHHNC in our patient is similar to that of p.(G191R).

5. Conclusions

In summary, the present study reports the clinical data of three patients diagnosed with FHHNC. The clinical diagnosis was confirmed by genetic analysis. Two novel mutations were identified, one in the *CLDN16* gene, c.602G > A; p.(G201E), and another in the *CLDN19* gene, c.388G > T; p.(G130C). Bioinformatics analysis suggested that the amino acid substitutions predicted for these mutations are pathogenic. In addition, functional analysis indicated that mutation c.388G > T also induces the skipping of exon 2 in *CLDN19* pre-mRNA splicing. Therefore, we showed for the first time that an exonic *CLDN19* mutation could alter the splicing of pre-mRNA, producing drastic alterations in the claudin-19 protein structure and loss of function. We propose that both the amino acid change and the altered splicing are involved in the pathogenesis of this mutation. Consequently, our findings provide useful information for a precise diagnosis and family counseling.

Conflict of interest

The authors declare no conflicts of interest.

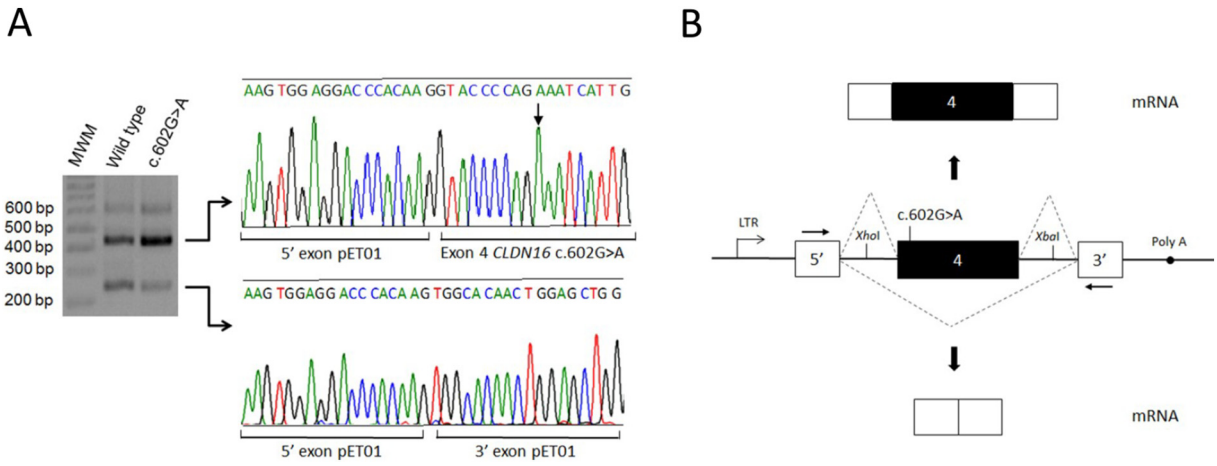

Fig. 3. Functional characterization of *CLDN16* exonic mutation c.602G > A using a minigene assay. (A) Agarose gel showing the results of the RT-PCR analysis of spliced transcripts expressed from *CLDN16* minigenes containing WT and mutant exons. Both mutant and WT minigenes generated mRNA products of the same size, a major band corresponding to the splicing and joining of *CLDN16* exon 4 and the two pET01 exons, and two alternative products (one smaller and one larger). The panel on the right shows electropherograms of two of the splicing products (we were unable to obtain the sequence of the larger minor product). The electropherogram on the top shows the joining of 5′ exon from vector pET01 with *CLDN19* exon 4 from mutant c.602G > A major product. The arrow indicates the corresponding mutation. The electropherogram on the bottom reveals the joining of 5′ and 3′ exons of vector pET01 in the smaller splicing product, and the skipping of exon 4. MWM, molecular weight marker. (B) Schematic representation of *CLDN16* minigene and of pre-mRNA splicing in both WT and mutant minigenes. Black and white boxes represent *CLDN19* exon 4 and pET01 exons, respectively. The position of mutations c.602G > A is indicated together with the restriction sites used for the construction of the minigenes. Dotted lines indicate the splice sites used in each case. Arrows above and below the white boxes represent primers used in the RT-PCR assays. The pET01 vector contains the long terminal repeat promoter (LTR) of Rous sarcoma virus and a polyadenylation site (Poly A).

Acknowledgements

We thank the families for their participation in this study. This work is part of the RenalTube project and was supported by grants PI14/00760 and PI17/00153 integrated in the *Plan Nacional de I+D+I 2013–2016* and co-financed by the ISCIII-Subdirección General de Evaluación y Fomento de la Investigación (Spain) and the European Regional Development Fund (European Union) “Another way to build Europe”. We are grateful to other members of the RenalTube group for their cooperation in the study: H. Gil-Peña, V. M. García-Nieto, H. González-Acosta, E. Córdoba-Lanus, A. García Castaño, E. Braga, E. Coto, E. García, F. Ángel Ordóñez, F. Santos, G. Pérez de Nanclares, J. Rodríguez, L. Castaño, L. Madariaga, M. I. Luis-Yanes, N. Mejía, R. Fuente, V. Álvarez, V. Loredo. GA y FCM are founder members of the Renaltube network. Part of this work was presented at the European Society of Human Genetics 2017 Conference, Copenhagen, Denmark, and the 1st International Caparica Conference in Splicing - SPLICING 2016, Caparica, Portugal.

References

Adzhubei, I.A., Schmidt, S., Peshkin, L., Ramensky, V.E., Gerasimova, A., Bork, P., Kondrashov, A.S., Sunyaev, S.R., 2010. A method and server for predicting damaging missense mutations. Nat. Methods 7 (4), 248–249. https://doi.org/10.1038/nmeth0410-248.

Bardet, C., Courson, F., Wu, Y., Khaddam, M., Salmon, B., Ribes, S., Thumfart, J., Yamaguti, P.M., Rochefort, G.Y., Figueres, M.L., Breiderhoff, T., Garcia-Castaño, A., Vallée, B., Le Denmat, D., Baroukh, B., Guilbert, T., Schmitt, A., Massé, J.M., Bazin, D., Lorenz, G., Morawietz, M., Hou, J., Carvalho-Lobato, P., Manzanares, M.C., Fricain, J.C., Talmud, D., Demontis, R., Neves, F., Zenaty, D., Berdal, A., Kiesow, A., Petzold, M., Menashi, S., Linglart, A., Acevedo, A.C., Vargas-Poussou, R., Müller, D., Houillier, P., Chaussain, C., 2016. Claudin-16 deficiency impairs tight junction function in ameloblasts, leading to abnormal enamel formation. J. Bone Miner. Res. 31 (3), 498–513. https://doi.org/10.1002/jbmr.2726.

Blanchard, A., Jeunemaitre, X., Coudol, P., Dechaux, M., Froissart, M., May, A., Demontis, R., Fournier, A., Paillard, M., Houillier, P., 2001. Paracellin-1 is critical for magnesium and calcium reabsorption in the human thick ascending limb of Henle. Kidney Int. 59 (6), 2206–2215. https://doi.org/10.1046/j.1523-1755.2001.00736.x.

Claverie-Martin, F., 2015. Familial hypomagnesaemia with hypercalciuria and nephrocalcinosis: clinical and molecular characteristics. Clin. Kidney J. 8 (6), 656–664. https://doi.org/10.1093/ckj/sfv081.

Claverie-Martín, F., García-Nieto, V., Loris, L., Ariceta, G., Nadal, I., Espinosa, L., Fernández-Maseda, A., Antón-Gamero, M., Avila, A., Madrid, A., González-Acosta, H., Córdoba-Lanus, E., Santos, F., Gil-Calvo, M., Espino, M., García-Martinez, E., Sanchez, A., Muley, R., RenalTube Group, 2013. Claudin-19 mutations and clinical phenotype in Spanish patients with familial hypomagnesemia with hypercalciuria and nephrocalcinosis. PLoS One 8 (1), e53151. https://doi.org/10.1371/journal.pone.0053151. (Correction in: PLoS One. 2013; 8(10): 10.1371/annotation/25732fb0-ae38-40f6-b8c6-eb4ba94ac996).

Claverie-Martín, F., Vargas-Poussou, R., Müller, D., García-Nieto, V., 2015. Clinical utility gene card for: familial hypomagnesemia with hypercalciuria and nephrocalcinosis with/without severe ocular involvement. Eur. J. Hum. Genet. 23 (6), 889. https://doi.org/10.1038/ejhg.2014.176.

de Calais, F.L., Smith, L.D., Raponi, M., Maciel-Guerra, A.T., Guerra-Junior, G., de Mello, M.P., Baralle, D., 2017. A study of splicing mutations in disorders of sex development. Sci. Rep. 7 (1), 16202. https://doi.org/10.1038/s41598-017-16296-3.

Desmet, F.O., Hamroun, D., Lalande, M., Collod-Béroud, G., Claustres, M., Béroud, C., 2009. Human Splicing Finder: an online bioinformatics tool to predict splicing signals. Nucleic Acids Res. 37 (9), e67. https://doi.org/10.1093/nar/gkp215.

Godron, A., Harambat, J., Boccio, V., Mensire, A., May, A., Rigothier, C., Couzi, L., Barrou, B., Godin, M., Chauveau, D., Faguer, S., Vallet, M., Cochat, P., Eckart, P., Guest, G., Guigonis, V., Houillier, P., Blanchard, A., Jeunemaitre, X., Vargas-Poussou, R., 2012. Familial hypomagnesemia with hypercalciuria and nephrocalcinosis: phenotype–genotype correlation and outcome in 32 patients with CLDN16 or CLDN19 mutations. Clin. J. Am. Soc. Nephrol. 7 (5), 801–809. https://doi.org/10.2215/CJN.12841211.

Gonzalez-Paredes, F.J., Ramos-Trujillo, E., Claverie-Martin, F., 2016. Three exonic mutations in polycystic kidney disease-2 gene (PKD2) alter splicing of its pre-mRNA in a minigene system. Gene 578 (1), 117–123. https://doi.org/10.1016/j.gene.2015.12.019.

Günzel, D., Yu, A.S., 2013. Claudins and the modulation of tight junction permeability. Physiol. Rev. 93 (2), 525–569. https://doi.org/10.1152/physrev.00019.2012.

Hampson, G., Konrad, M.A., Scoble, J., 2008. Familial hypomagnesaemia with hypercalciuria and nephrocalcinosis (FHHNC): compound heterozygous mutation in the claudin 16 (CLDN16) gene. BMC Nephrol. 9, 12. https://doi.org/10.1186/1471-2369-9-12.

Hanssen, O., Castermans, E., Bovy, C., Weekers, L., Erpicum, P., Dubois, B., Bours, V., Krzesinski, J.M., Jouret, F., 2014. Two novel mutations of the CLDN16 gene cause familial hypomagnesaemia with hypercalciuria and nephrocalcinosis. Clin. Kidney J. 7 (3), 282–285. https://doi.org/10.1093/ckj/sfu019.

Hou, J., Renigunta, A., Konrad, M., Gomes, A.S., Schneeberger, E.E., Paul, D.L., Waldegger, S., Goodenough, D.A., 2008. Claudin-16 and claudin-19 interact and form a cation-selective tight junction complex. J. Clin. Invest. 118 (2), 619–628. https://doi.org/10.1172/JCI33970.

Hou, J., Renigunta, A., Gomes, A.S., Hou, M., Paul, D.L., Waldegger, S., Goodenough, D.A., 2009. Claudin-16 and claudin-19 interaction is required for their assembly into tight junctions and for renal reabsorption of magnesium. Proc. Natl. Acad. Sci. U. S. A. 106 (36), 15350–15355. https://doi.org/10.1073/pnas.0907724106.

Konrad, M., Schaller, A., Seelow, D., Pandey, A.V., Waldegger, S., Lesslauer, A., Vitzthum, H., Suzuki, Y., Luk, J.M., Becker, C., Schlingmann, K.P., Schmid, M., Rodriguez-Soriano, J., Ariceta, G., Cano, F., Enriquez, R., Juppner, H., Bakkaloglu, S.A., Hediger, M.A., Gallati, S., Neuhauss, S.C., Nurnberg, P., Weber, S., 2006. Mutations in the tight-junction gene claudin 19 (CLDN19) are associated with renal magnesium

wasting, renal failure, and severe ocular involvement. Am. J. Hum. Genet. 79 (5), 949–957. https://doi.org/10.1086/508617.
Konrad, M., Hou, J., Weber, S., Dötsch, J., Kari, J.A., Seeman, T., Kuwertz-Bröking, E., Peco Antic, A., Tasic, V., Dittrich, K., Alshaya, H.O., von Vigier, R.O., Gallati, S., Goodenough, D.A., Schaller, A., 2008. CLDN16 genotype predicts renal decline in familial hypomagnesemia with hypercalciuria and nephrocalcinosis. J. Am. Soc. Nephrol. 19 (1), 171–181. https://doi.org/10.1681/ASN.2007060709.
Martin-Nuñez, E., Cordoba-Lanus, E., Gonzalez-Acosta, H., Oliet, A., Izquierdo, E., Claverie-Martin, F., 2015. Haplotype analysis of CLDN19 single nucleotide polymorphisms in Spanish patients with familial hypomagnesemia with hypercalciuria and nephrocalcinosis. World J. Pediatr. 11 (3), 272–275. https://doi.org/10.1007/s12519-014-0528-3.
Michelis, M.F., Drash, A.L., Linarelli, L.G., De Rubertis, F.R., Davis, B.B., 1972. Decreased bicarbonate threshold and renal magnesium wasting in a sibship with distal renal tubular acidosis. (Evaluation of the pathophysiological role of parathyroid hormone). Metabolism 21 (10), 905–920. https://doi.org/10.1016/0026-0495(72)90025-X.
Miyamoto, T., Morita, K., Takemoto, D., Takeuchi, K., Kitano, Y., Miyakawa, T., Nakayama, K., Okamura, Y., Sasaki, H., Miyachi, Y., Furuse, M., Tsukita, S., 2005. Tight junctions in Schwann cells of peripheral myelinated axons: a lesson from claudin-19-deficient mice. J. Cell Biol. 169 (3), 527–538. https://doi.org/10.1083/jcb.200501154.
Müller, D., Kausalya, P.J., Claverie-Martin, F., Meij, I.C., Eggert, P., Garcia-Nieto, V., Hunziker, W., 2003. A novel claudin 16 mutation associated with childhood hypercalciuria abolishes binding to ZO-1 and results in lysosomal mistargeting. Am. J. Hum. Genet. 73 (6), 1293–1301. https://doi.org/10.1086/380418.
Naeem, M., Hussain, S., Akhtar, N., 2011. Mutation in the tight-junction gene claudin 19 (CLDN19) and familial hypomagnesemia, hypercalciuria, nephrocalcinosis (FHHNC) and severe ocular disease. Am. J. Nephrol. 34 (3), 241–248. https://doi.org/10.1159/000330854.
Pejaver, V., Urresti, J., Lugo-Martinez, J., Pagel, K.A., Lin, G.N., Nam, H., Mort, M., Cooper, D.N., Sebat, J., Iakoucheva, L.M., Mooney, S.D., Radivojac, P., 2017. MutPred2: inferring the molecular and phenotypic impact of amino acid variants. bioRxiv, 134981. https://doi.org/10.1101/134981.
Praga, M., Vara, J., González-Parra, E., Andrés, A., Alamo, C., Araque, A., Ortiz, A., Rodicio, J.L., 1995. Familial hypomagnesemia with hypercalciuria and nephrocalcinosis. Kidney Int. 47 (5), 1419–1425. https://doi.org/10.1038/ki.1995.199.
Reese, M.G., Eeckman, F.H., Kulp, D., Haussler, D., 1997. Improved splice site detection in genie. J. Comput. Biol. 4 (3), 311–323. https://doi.org/10.1089/cmb.1997.4.311.
Roy, A., Kucukural, A., Zhang, Y., 2010. I-TASSER: a unified platform for automated protein structure and function prediction. Nat. Protoc. 5 (4), 725–738. https://doi.org/10.1038/nprot.2010.5.
Schwartz, G.J., Muñoz, A., Schneider, M.F., Mak, R.H., Kaskel, F., Warady, B.A., Furth, S.L., 2009. New equations to estimate GFR in children with CKD. J. Am. Soc. Nephrol. 20 (3), 629–637. https://doi.org/10.1681/ASN.2008030287.
Sim, N.L., Kumar, P., Hu, J., Henikoff, S., Schneider, G., Ng, P.C., 2012. SIFT web server: predicting effects of amino acid substitutions on proteins. Nucleic Acids Res. 40, W452–W457. https://doi.org/10.1093/nar/gks539. (Web Server issue).
Simon, D.B., Lu, Y., Choate, K.A., Velazquez, H., Al-Sabban, E., Praga, M., Casari, G., Bettinelli, A., Colussi, G., Rodriguez-Soriano, J., McCredie, D., Milford, D., Sanjad, S., Lifton, R.P., 1999. Paracellin-1, a renal tight junction protein required for paracellular Mg^{2+} resorption. Science 285 (5424), 103–106. https://doi.org/10.1126/science.285.5424.103.
Steffensen, A.Y., Dandanell, M., Jønson, L., Ejlertsen, B., Gerdes, A.M., Nielsen, F.C., Hansen, Tv, 2014. Functional characterization of BRCA1 gene variants by mini-gene splicing assay. Eur. J. Hum. Genet. 22, 1362–1368. https://doi.org/10.1038/ejhg.2014.40.
Stenson, P.D., Mort, M., Ball, E.V., Evans, K., Hayden, M., Heywood, S., Hussain, M., Phillips, A.D., Cooper, D.N., 2017. The Human Gene Mutation Database: towards a comprehensive repository of inherited mutation data for medical research, genetic diagnosis and next-generation sequencing studies. Hum. Genet. 136 (6), 665–677. https://doi.org/10.1007/s00439-017-1779-6.
Suarez-Artiles, L., Perdomo-Ramirez, A., Ramos-Trujillo, E., Claverie-Martin, F., 2018. Splicing analysis of exonic OCRL mutations causing Lowe syndrome or dent-2 disease. Genes (Basel) 9 (1). https://doi.org/10.3390/genes9010015. (pii: E15).
Tavtigian, S.V., Deffenbaugh, A.M., Yin, L., Judkins, T., Scholl, T., Samollow, P.B., de Silva, D., Zharkikh, A., Thomas, A., 2006. Comprehensive statistical study of 452 BRCA1 missense substitutions with classification of eight recurrent substitutions as neutral. J. Med. Genet. 43 (4), 295–305. https://doi.org/10.1136/jmg.2005.033878.
Tournier, I., Vezain, M., Martins, A., Charbonnier, F., Baert-Desurmont, S., Olschwang, S., Wang, Q., Buisine, M.P., Soret, J., Tazi, J., Frébourg, T., Tosi, M., 2008. A large fraction of unclassified variants of the mismatch repair genes MLH1 and MSH2 is associated with splicing defects. Hum. Mutat. 29 (12), 1412–1424. https://doi.org/10.1002/humu.20796.
Tsukita, S., Furuse, M., 2000. Pores in the wall: claudins constitute tight junction strands containing aqueous pores. J. Cell Biol. 149 (1), 13–16.
van der Klift, H.M., Jansen, A.M., van der Steenstraten, N., Bik, E.C., Tops, C.M., Devilee, P., Wijnen, J.T., 2015. Splicing analysis for exonic and intronic mismatch repair gene variants associated with Lynch syndrome confirms high concordance between minigene assays and patient RNA analyses. Mol. Genet. Genomic Med. 3 (4), 327–345. https://doi.org/10.1002/mgg3.145.
Weber, S., Hoffmann, K., Jeck, N., Saar, K., Boeswald, M., Kuwertz-Broeking, E., Meij, I.C., Knoers, N.V., Cochat, P., Suláková, T., Bonzel, K.E., Soergel, M., Manz, F., Schaerer, K., Seyberth, H.W., Reis, A., Konrad, M., 2000. Familial hypomagnesaemia with hypercalciuria and nephrocalcinosis maps to chromosome 3q27 and is associated with mutations in the PCLN-1 gene. Eur. J. Hum. Genet. 8, 414–422. https://doi.org/10.1038/sj.ejhg.5200475.
Weber, S., Schneider, L., Peters, M., Misselwitz, J., Rönnefarth, G., Böswald, M., Bonzel, K.E., Seeman, T., Suláková, T., Kuwertz-Bröking, E., Gregoric, A., Palcoux, J.B., Tasic, V., Manz, F., Schärer, K., Seyberth, H.W., Konrad, M., 2001. Novel paracellin-1 mutations in 25 families with familial hypomagnesemia with hypercalciuria and nephrocalcinosis. J. Am. Soc. Nephrol. 12 (9), 1872–1881.
Yamaguti, P.M., Neves, F.A., Hotton, D., Bardet, C., de La Dure-Molla, M., Castro, L.C., Scher, M.D., Barbosa, M.E., Ditsch, C., Fricain, J.C., de La Faille, R., Figueres, M.L., Vargas-Poussou, R., Houillier, P., Chaussain, C., Babajko, S., Berdal, A., Acevedo, A.C., 2017. Amelogenesis imperfecta in familial hypomagnesaemia and hypercalciuria with nephrocalcinosis caused by CLDN19 gene mutations. J. Med. Genet. 54 (1), 26–37. https://doi.org/10.1136/jmedgenet-2016-103956.
Yang, J., Yan, R., Roy, A., Xu, D., Poisson, J., Zhang, Y., 2015. The I-TASSER suite: protein structure and function prediction. Nat. Methods 12 (1), 7–8. https://doi.org/10.1038/nmeth.3213.